1	Application of electrical resistivity to map the stratigraphy and salinity of fluvio-deltaic aquifers:					
2	case studies from Bangladesh reveal promises and pitfalls					
3	Micaela N. Pedrazas <sup>1</sup> *, M. Bayani Cardenas <sup>1</sup> , Alamgir Hosain <sup>2</sup> , Cansu Demir <sup>1</sup> , Kazi Matin Ahmed <sup>3</sup> , Syed					
4	Humayun Akhter <sup>3</sup> , Lichun Wang <sup>4</sup> , Saugata Datta <sup>5</sup> , and Peter S. K. Knappett <sup>6</sup>					
5	1. Dept. of Geological Sciences, The University of Texas at Austin					
6	2. Dept. of Coastal Studies and Disaster Management, University of Barisal					
7	3. Dept. of Geology, University of Dhaka					
8	4. Institute of Surface-Earth System Science, School of Earth System Science, Tianjin University					
9	5. Dept. of Geological Sciences, University of Texas at San Antonio					
10	6. Dept. of Geology & Geophysics, Texas A&M University					
11	*corresponding author: mpedrazash@utexas.edu					
12	Abstract					
13	Fluvio-deltaic aquifers are the primary source of drinking water for the people of Bangladesh.					
14	Such aquifers, which comprise the Ganges-Brahmaputra-Meghna Delta, are extremely hydrogeologically					
15	heterogeneous. Because of widespread groundwater quality issues in Bangladesh, it is crucial to know the					
16	hydrostratigraphic architecture and hydrochemistry of the aquifers as some units are contaminated					
17	whereas others are safe. Geophysical methods provide a potentially effective and non-invasive method for					
18	extensive characterization of these aquifers. This study applies and investigates the limitations of using					
19	electrical resistivity imaging (ERI) for mapping the hydrostratigraphy and salinity of an aquifer-aquitard					
20	system adjacent to the Meghna River. Some ER sections showed excellent correlation between resistivity					
21	and grain size. These suggest that ERI is a powerful tool for mapping internal aquifer architecture and					
22	their boundaries with finer-grained aquitards which clearly appear as low ER zones. However, in parts of					
23	some ER sections, variations in electrical properties were determined by porewater resistivity. In these					
24	cases, low ER was indicative of brine and did not indicate the presence of finer-grained materials such as					
25	silt or clay. Accordingly, the following hydrostratigraphic zones with different resistivities were detected:					
26	(1) aquifers saturated with fresh ground water, (2) a regional silt/clay aquitard, and (3) a deeper brine-					

saturated formation. In addition, shallow silt/clay pockets were detected close to the river and below the vadose zone. ERI is thus a promising technique for mapping aquifers versus aquitards. However, the observations are easily confounded by porewater salinity. In such cases, borehole information and groundwater salinity measurements are necessary for ground-truthing.

**Key words:** electrical resistivity; Bangladesh; hydrostratigraphy; geophysical methods; groundwater exploration

33

34

35

36

37

38

39

40

41

42

43

44

45

46

47

48

49

50

51

52

27

28

29

30

31

32

#### 1. Introduction

South and Southeast Asia, and in particular Bangladesh, rely heavily on groundwater as the main drinking water supply (~80%), and as a means of poverty alleviation through farm-land irrigation (Zahid and Ahmed, 2006). However, over-exploitation of the Bengal Basin aquifers during the last decade has resulted in a reduction of groundwater storage by 32% between 2003-2013 (Khaki, et al., 2018). Compounding this groundwater depletion, widespread arsenic (As) poisoning of shallow aquifers derived from the reduction of As-rich Fe-oxyhydroxides is well known in the region (Datta, et al., 2011, Nickson, et al., 1998). The challenge of identifying and solving these groundwater resource issues is bedeviled by the ubiquitous problem of aquifer heterogeneity. Preferential flow and fast flow paths for contaminant transport to deeper aquifers are present (Michael and Khan, 2016). This obscures the prediction of which aquifers are vulnerable to ingress of dissolved As through breaks in clay layers (Mozumder, et al., 2020) or the in-situ release of As by reductive dissolution of iron oxides by dissolved organic carbon (DOC) drawn from clay layers under the influence of depressurization of low-As aquifers (Mihajlov, et al., 2020). First-order information regarding sedimentary architecture such as the spatial extent and thickness of hydrogeologic units is necessary to mitigate contamination risks and resource issues. However, an indepth understanding of the continuity of hydrostratigraphic units, connections with surface water bodies, and porewater salinity distribution can be difficult to obtain.

There is a pressing need to advance the understanding of the fluvio-deltaic aquifer-aquitard system along the Meghna River in Bangladesh. Many villages are found along the banks of the Meghna.

In Bangladesh, despite the relatively cheap cost of drilling wells by western standards, the expenses are still prohibitive for locals especially those relying on private wells for domestic water use. Hence, for the millions of privately owned wells, groundwater exploration is usually not exercised with extensive mapping. Direct observations made through drilling are sparse, expensive and provide only limited point observations of lithology and groundwater salinity.

Electrical resistivity imaging (ERI) is a cost-effective near-surface geophysical method that can image the electrical properties of aquifers and water stored within its pores (Daily, et al., 1992). With ERI, an electrical current is injected into the subsurface using electrodes buried just beneath the surface. The voltaic response of the subsurface materials is then recorded by potential electrodes while the electrical current is active. The technique is useful for groundwater applications because the electrical resistivity of porous media is controlled by multiple geological and pore-fluid properties such as porosity, pore-water salinity, fluid saturation, soil texture, overburden pressure, temperature, and electrical surface properties of the grain matrix (Cai et al., 2017, Loke, 2011). In shallow fluvio-deltaic aquifers, below the water table, where the overburden pressure and water saturation are more or less static, ERI is particularly sensitive to the resistivity contrasts between aquifers (relatively coarser sediment) and aquitards (relatively finer sediment) as well as porewater resistivity. Thus, ERI can potentially discriminate between freshwater aquifers, brine saturated aquifers, and aquitards. Under optimal conditions, ERI can possibly map sub-units with different textures and thus hydrologic properties within aquifers.

In Bangladesh, a few studies have determined empirical relationships between bulk electrical resistivity and solute concentrations and geotechnical properties, as well as qualitative relationships between lithology and resistivity (Hossain, 2016, Kabir, et al., 2011, Woobaidullah, et al., 2008). In other parts of the world, electrical resistivity has been used to delineate and monitor salt water intrusion into fresh water aquifers (Adepelumi, et al., 2009, De Franco, et al., 2009, Nowroozi, et al., 1999). This manuscript reports on a few case studies which further reveal the promises and pitfalls of ERI for integrated hydrostratigraphic and hydrochemical characterization of an aquifer-aquitard system along the Meghna River. The goal of our study is to illustrate how well (or not) ERI can work in the context of

Bangladesh's fluvio-deltaic sedimentary aquifers in terms of its ability to distinguish aquifer physical and hydrochemical properties.

#### 2. Background on the study area

The Bengal Basin encompassing major parts of Bangladesh and its neighboring regions is a result of the collision of India with Eurasia and concomitant filling of the basin with sediment derived from erosion of mountains and uplands and transported and deposited by the Ganges and Brahmaputra Rivers to where the Bay of Bengal once existed (Najman, et al., 2008). The end result is a thick sedimentary sequence that starts in the northern part of Bangladesh near Sylhet, where it is tens of meters thick, and reaches up to 20 km at the modern shoreward limit of the Ganges-Brahmaputra-Meghna River Delta complex (Alam, et al., 2003). The Meghna River is the third largest river amongst the three in terms of annual volumetric discharge. It flows from North to South and merges other major rivers before it empties into the Bay of Bengal.

The upper portions of the Bay of Bengal is filled with a Quaternary alluvial sequence deposited by the Ganges and Brahmaputra Rivers (Wilson and Goodbred, 2015). Broadly, there are two distinct aquifers within this sequence- A shallow aquifer comprised of fine sands that is sometimes capped by a grey colored clay/silt blanket and a deeper aquifer comprised of medium to coarse sands. These two aquifers are separated by a relatively impermeable silt/clay layer (Islam, et al., 2018) which is widely present across the Bengal Basin (McArthur, et al., 2008) and near the Meghna River (Knappett, et al., 2016, Mozumder, et al., 2020).

The study focused on a site that is approximately 30 km east of the capital city of Dhaka. Areas within tens to hundreds of meters of the Meghna River were studied to map the structure of the shallow, high-As aquifer, and the continuity of the clay layer separating this aquifer from the underlying, generally low-As aquifer. Broadly, two study transects were established. The North and South transects are roughly 12 km apart along the river (Fig. 1). Electrical resistivity surveys were conducted in the North transect subsets in January 2016, including its West and East subset surveys which were on opposite banks of the south-flowing Meghna River. The surveys in the South transects were conducted in January 2020.

#### 3. Methods

## 3.1. Electrical resistivity imaging and processing

An eight-channel ERI instrument (SuperSting R8, Advanced Geosciences, Inc.) with 84 electrodes was used for all surveys. When acquiring ERI surveys, there exists a tradeoff between depth and resolution, which is controlled by the spacing between electrodes buried in the ground. Thus, different spacing arrangement were used for the surveys in order to acquire information at varying depths. In January 2016, four surveys 498 m long were acquired using the dipole-dipole array configuration and 6 m electrode spacing to investigate down to 100 m depth at the North, East and West study transects. In January 2020, the dipole-dipole array configuration was used with 1.5 m and 3 m electrode spacing to investigate the near-surface shallow aquifer at a higher resolution at the South study transects (Fig. 1). To further distinguish the individual surveys, they are referred to by appending to their locations, e.g., North vs South, whether the transect is perpendicular or parallel to the river and a number when there is more than one. A final name for example is "South Perpendicular 1". This identification convention is followed throughout the manuscript. The individual transects are shown in Fig. 1.

The ER data were processed and inverted using RES2DINV version 4.9.11 (Loke, 2006) to obtain a subsurface resistivity distribution tomogram. All data were inverted using the robust inversion constraint and the finite-element method to minimize the root-mean square (RMS) error difference between the measured and modeled apparent resistivity values. The robust inversion constraint was chosen to better resolve the expected presence of sand/silt (aquifer/aquitard) contacts. The parameters used in the inversion are presented in Table 1. Additional post-processing steps, e.g., visualization, extraction of profiles, and statistical analyses, were conducted in the MATLAB program.

# 3.2. Direct observations of subsurface materials during well drilling: borehole data

Local drillers were hired to install deep piezometers and to obtain borehole cuttings. The drilling was performed using the local hand-flapper drilling method based on the application of suction and its release using the hand as a check valve to a PVC pipe (Horneman, et al., 2004). As the pipe was lowered, sediment slurry was collected at every ~1.5 m intervals, and was immediately inspected for visual

identification of the dominant grain size category. At each location, a cluster of three wells were drilled to different depths. Each well was screened at 1.5 m from the bottom. After well development and appropriate purging, the electrical conductivity of the groundwater was measured using a calibrated, handheld fluid electrical conductivity probe (YSI Professional Plus) at the boreholes from East, West and South sites. Using a peristaltic pump, groundwater was actively pumped from the well into a small and continuously overflowing container wherein the probe was submerged. The nearest or overlapping borehole data was used in the interpretation for constraining the estimated bulk resistivity resulting from the processed ERI data. Fig. 1 shows the spatial distribution of the borehole data.

# 3.3. Calculation of theoretical bulk resistivity

Results of ERI can be interpreted by calculating the expected theoretical values for specific combinations of sediment and porewater properties. These properties represent the hydrologic and hydrochemical properties of the aquifer. Archie's Law relates all these properties (Archie, 1942). It is the petrophysical relationship between bulk resistivity  $(\rho_b)$ , fluid resistivity  $(\rho_w)$ , sediment porosity  $(\phi)$ , and fluid saturation  $(S_w)$ :

$$\rho_b = a\phi^{-m}S_w^{-n}\rho_w$$

Thus, if the parameters in Archie's Law are known, one can determine the expected  $\rho_b$  values. Archie's Law can also be used in inverse applications where if the  $\rho_b$  is known, e.g., from inverted ERI data (or ER tomograms), one could potentially determine any one of the parameters in Archie's Law if the others are known or sufficiently constrained. In this study, expected  $\rho_b$  values were calculated and qualitatively compared with the observations. The following assumptions were considered: (1) the tortuosity factor  $a=\phi^{1/2}$  (Bruggeman, 1935); (2) the sediment is fully saturated below the water table ( $S_w=1$ ; the water table is typically no deeper than 2-3 m in the study transects); (3) the fluid resistivity ( $\rho_w$ ) at discrete groundwater sampling depths is known following measurements; (4) the cementation factor m=1.983 (Pearson, et al., 1983); and finally, (5) porosity  $\phi$  was assessed from the minimum for unconsolidated sand and gravel (20%) and the maximum for clay (60%) following typical values these sediment (Fetter,

156 1994).

The classical Archie's Law provides preliminary theoretical estimates of  $\rho_b$ . It ignores electrical conduction through the solid surface of the matrix and assumes current mainly passes through the fluid. Grain surface conduction of electrical currents may be important when clay minerals are present (Wang and Revil, 2020, Cai, et al., 2017, Glover, et al., 2000; Waxman and Smits, 1968).

#### 4. Results and Discussion

## 4.1. Shallow ER surveys: South transects

The South transects imaged down to ~30 m for the river-perpendicular surveys and to 50 m for the river-parallel survey (Fig. 2b). For the perpendicular surveys, away from the river and at higher elevation, there is a 2 m-thick very resistive (> 316  $\Omega$ m) zone. This corresponds to the vadose zone. All transects showed a similar subsurface general resistivity distribution trend. This can be seen from vertical profiles of resistivity extracted from the middle of each tomogram (Fig. 2a). From top to bottom, there were five distinct resistivity zones: (1) a resistive (> 75  $\Omega$ m) but heterogeneous ~2.5 m thick zone spanning across the top of the survey transects, (2) an intermediate conductive zone (> 31.6  $\Omega$ m and < 75  $\Omega$ m) of approximately 6 m in thickness, (3) a 12 m thick resistive layer that becomes most resistive at its vertical center, (4) a ~4 m thick gradually changing resistive layer ranging from a high of ~90  $\Omega$ m at approximately 20 m depth to < 30  $\Omega$ m below 24 m, and a (5) homogeneous low resistivity zone that continually decreased in resistivity with depth. The southern transects did not image the base of the least resistive bottom material. There were pockets of less resistive sediment within the intermediate resistive layer predominantly below the vadose zone and closest to the river.

#### 4.2. Deep ER surveys: North, West, and East transects

The North, West and East transects were imaged down to 100 m (Fig. 3b). The perpendicular North transect showed a 2 m-thick very resistive vadose zone layer that extends for 60 m across the survey starting at about 60 m away from the river, similar to the South perpendicular transects. All transects showed a similar general resistivity pattern illustrated further by the vertical resistivity profiles extracted from the middle of each survey, but with some exceptions (Fig. 3a). The uppermost 40 m of the

deep surveys agreed with the results from the higher resolution shallow surveys with the exception of the West parallel survey. In the latter's case, there were more conductive materials in the top 10 m. In the North transects it became slightly more resistive with depth below 40 m, whereas within the West parallel transect, the resistivity was constantly at 31.6  $\Omega$ m down to 80 m and then it became slightly more conductive deeper. The East parallel survey results differed markedly from the rest; there was a very conductive layer below 40 m down to 100 m in the East transect.

# 4.3. Vertical distribution of fluid resistivity from well sampling

There were obvious variations in salinity within and across borehole locations. The East borehole (Fig. 4a) showed systematic increase in salinity with depth, with the pore fluid becoming very conductive ( $\sim 5~\Omega m$  or 2108  $\mu S/cm$ ) down to about 70 m yet borehole cuttings did not indicate the presence of clay at any depths at which fluid resistivity was assessed. The West borehole showed moderate salinity variations with depth (Fig. 4b), increasing in resistivity by 6  $\Omega m$  at 46 m depth and then decreasing slightly by 2  $\Omega m$  at 61 m where clay cuttings were observed. The shallower South boreholes showed hardly any salinity variations with depth, with fluid resistivity remaining at approximately 30  $\Omega m$  throughout the vertical profile even though clay cuttings were present at some depths where fluid resistivity was assessed (Fig. 4c and 4d).

#### 4.4. Grainsize and lithological variations

Detailed lithology was logged during drilling only in the South transects where cuttings in the form of a sediment slurry were retrieved and visually assessed for grainsize at the site itself. There were two boreholes co-located along the South-perpendicular 2 survey line (BH-1 and BH-2), with the deeper of these two (BH-2) located at the intersections between the South – perpendicular 2 and South- parallel surveys (Fig. 1c). There is a general agreement between coarser grainsize and higher resistivity values. The grainsize log, when overlaid on top of the South tomograms, shows agreement of depth intervals with coarser grain size and higher resistivity values (Fig. 5). Furthermore, the combination of the tomograms (Fig. 5c) shows consistency across the different neighboring or overlapping transects, and thus continuity of the different zones. Cuttings from the other boreholes (East and West) were simply described as fine

(silt/clay) or coarse materials (sand). The results of this binary description are shown in Fig. 4.

208

209

210

211

212

213

214

215

216

217

218

219

220

221

222

223

224

225

226

227

228

229

230

231

232

233

# 4.5. Constraining the inverted electrical resistivity tomograms with fluid resistivity and grainsize information

The combination of some fluid resistivity measurements and borehole lithology allows for constraining the ER tomograms. To analyze the relationship between grainsize and resistivity, vertical resistivity profiles were extracted from the tomograms at the borehole locations. These resistivity values were paired with the grainsize groups observed at their corresponding depths (Fig. 5). The groups are: (i) clay, (ii) silt to very fine sand, (iii) fine to medium sand, and (iv) coarse to very coarse sand. A statistical comparison was then performed to determine if each grainsize group has a unique resistivity signature. Given the low sample numbers, a t-test statistic was used to evaluate if the groups had different means relative to each other. The t-test p-values (the probability of concluding that the groups have different means when they do not) showed that all the groups have different means at a 10% significance level (p<0.10) and that almost all groups are also differentiable at the 5% significance level (p<0.05) (Table 2). The only exception is the marginally significant (p=0.054) difference in resistivity values for fine/medium sand and coarse/very coarse. The ability to distinguish between unique grainsize groups is further illustrated when visually comparing the statistical distributions (histograms) of resistivity for each group through 'violin plots'. The distinction between the different groups is visually apparent (Fig. 6). This indicates that at the South transects ERI is able to constrain the texture of the aquifer sediment (stratigraphic architecture) and also helps in the detection of the aquitards. The aquitard, comprised of silt and then finally clay was clearly detected underlying the aquifer at approximately 20 m depth.

Archie's Law was used to predict the expected bulk resistivity based on the observed lithology and fluid resistivity. The predicted values (shown as bars in Fig. 4) for the South transects (Fig. 4c and 4d) roughly overlap with those that were observed in extracted vertical ER profiles. However, the resistivity values extracted from the tomograms tended to be on the lower range of if not lower than the predicted values. Similar comparisons between predicted and inverted tomogram profile values were observed for the West (Fig. 4a) and East (Fig. 4b) cases. The comparisons were least similar for the

borehole close the West transect. This suggests that the porosity of the aquifer materials is smaller than the values used in Archie's law predictions, assuming that all other parameters were well-constrained. However, this is unlikely given that the typical range was already used in the theoretical calculations. There are a few potential explanations. First, the resistivity of the aquifer materials is smaller, i.e., there are conductive minerals. Second, the borehole is located approximately 200 m west of the ER transect and therefore may not be representative of the materials encountered within the coverage of the ER survey. Note that the borehole is offset from the ER transect (Fig. 1d). As such, some disagreement is not surprising.

# 4.6. Further interpretation and limitations

The shallow surveys with shorter electrode spacing at the South site produce higher resolution resistivity tomograms. The South transects also exhibited minimum porewater salinity variation with depth than at the other sites (Fig. 4). Thus, it was possible to correlate with and attribute the changes in resistivity to changes in sediment texture rather than fluid resistivity at the South transects. The lithological log at BH-2 correlated with the vertical resistivity profiles revealed that the first approximately 30 m from the top is comprised of sand (ranging from fine to medium sand) with a minor silt aquitard near the surface. This unconfined and semi-confined aquifer (owing to the minor intercalated silt) is underlain by a regional clay aquitard. Below this clay aquitard, the resistivity at the South site decreases until it reaches a value  $< 10 \ \Omega m$  at 50 m depth. The clay cuttings found at 31.5 m depth showed a resistivity of 20  $\Omega m$ ; thus, a resistivity  $< 10 \ \Omega m$  may be indicative of brine-saturated sediment.

The deeper boreholes in the East and West sites reveal that the upper horizon of the clay aquitard is located at a depth of  $\sim 30$  m and has a thickness of 6 m (East) and 12 m (West), followed by a deeper sandy aquifer and then another clay aquitard at a depth of  $\sim 60$  m (Fig. 4a and 4b). For the North transects, where no borehole information is available, the transition between the shallow resistive layer and the conductive zone corresponded to the depth at which clay was found in the South transects (Fig. 2). According to the ER tomogram, below the clay aquitard of varying thickness, there is resistive sediment that is most likely the deeper sandy aquifer observed in the East and West boreholes. The

conductive sediment below 30 m depth in the West and East tomograms is more difficult to interpret since in both sites the lithology log indicates a 20 m thick deep sandy aquifer between 40 - 60 m depth, which is apparent in the North ER tomograms, but this depth interval manifests as a conductive zone in the West and East tomograms. Integration of the fluid resistivities into the analysis suggests that the higher electrical conductivity for the West and, especially, the East surveys, results from the higher porewater salinity. At 70 m depth, the East transect fluid resistivity reaches 4  $\Omega$ m, indicative of more saline porewater. It seems that the clay aquitard with resistivity  $\sim$  30  $\Omega$ m is more resistive than brackish water-saturated sand < 10  $\Omega$ m. However, in the deep zones, it is difficult to pinpoint the depth at which the conductive clay layer transitions to more saline water-saturated sand without additional evidence from borehole cuttings. Had the fluid resistivity in these conductive zones been unknown, this zone could have been interpreted as an aquitard if the lessons and resistivity-grainsize correlations from the South transects were extrapolated to this location.

Our analysis and application of Archie's Law assumes that bulk resistivity variations due to the electrical properties of the solid matrix can be ignored. That is there is no electrical conduction through the surfaces of the grains. This assumption is violated when substantial clay minerals are present (Wang and Revil, 2020, Cai, et al., 2017, Glover, et al., 2000; Waxman and Smits, 1968). Unfortunately, our lithologic characterization is not sufficient to quantify the clay content, let alone the cation exchange capacity of the clays and the bulk material in general which is necessary for constraining surface conduction (Wang and Revil, 2020, Waxman and Smits, 1968). Nonetheless, future studies of fluviodeltaic aquifers with a mix of sand, silt, and clays should also consider petrophysical models which consider electrical conduction by the solid phase of the bulk sediment-water mixture, e.g., Glover et al. (2000) and Wang and Revil (2020).

## 5. Summary and Conclusions

This study reports on hydrogeophysical mapping of two main aquifers vertically separated by a clay aquitard in the fluvio-deltaic sediment sequence next to the Meghna River in Bangladesh. Overall, the electrical resistivity tomograms indicate the prevalence of these three zones or hydrostratigraphic

units. Going from top to bottom, these are: (1) a  $\sim$ 12-m thick freshwater bearing coarse sand aquifer capped by a silt layer, (2) a  $\sim$  10 m clay aquitard, and (3) a thick sandy aquifer with parts that are fresh and parts that are brine-saturated. When there is no strong variation in groundwater salinity, the electrical resistivity tomograms showed a strong correlation between resistivity and grainsize making electrical resistivity a powerful and efficient tool for hydrostratigraphic characterization. However, when substantial salinity variations are present, it is crucial to integrate fluid resistivity measurements to distinguish between the sediment and the porewater electrical signal. This is a major limitation to the broad application of the electrical resistivity imaging for physical mapping of aquifers. On the other hand, it also illustrates the potential to map hydrochemical variations at aquifer scales, but in this application it is the sediment properties that need to be constrained.

## Acknowledgements

MNP was supported by a fellowship from the Ivanhoe Foundation. This project was funded by the National Science Foundation (grants EAR-1852653, EAR-1940772 and EAR-1852652). Additional support was provided by the Geology Foundation of the University of Texas at Austin. We thank Imtiaz Choudhury, Abu Saeed Arman, Mesbah Uddin Bhuiyan, Rajib Mozumder, Kimberley Rhodes and Kimberley Myers for assistance with field work. MNP conducted the resistivity data processing, created the figures and wrote an initial draft of the manuscript with guidance from MBC. All authors participated in or provided input during fieldwork and the writing of the manuscript. All geophysical data are available in Hydroshare at <a href="https://doi.org/10.4211/hs.cf3c2633962b4121a231110d4be0d7a5">https://doi.org/10.4211/hs.cf3c2633962b4121a231110d4be0d7a5</a>. We thank two anonymous reviewers for their comments.

#### References

Adepelumi AA, Ako B, Ajayi T, Afolabi O, Omotoso E (2009) Delineation of saltwater intrusion into the freshwater aquifer of Lekki Peninsula, Lagos, Nigeria. Environmental Geology 56: 927-933

Alam M, Alam MM, Curray JR, Chowdhury MLR, Gani MR (2003) An overview of the sedimentary geology of the Bengal Basin in relation to the regional tectonic framework and basin-fill history. Sedimentary Geology 155: 179-208 DOI https://doi.org/10.1016/S0037-0738(02)00180-X

Archie GE (1942) The Electrical Resistivity Log as an Aid in Determining Some Reservoir Characteristics. SPE-942054-G 146: 54-62 DOI 10.2118/942054-G

- 315 Bruggeman DAG (1935) Berechnung verschiedener physikalischer Konstanten von heterogenen 316 Substanzen. I. Dielektrizitätskonstanten und Leitfähigkeiten der Mischkörper aus isotropen 317 Substanzen. Annalen der Physik 416: 636-664 DOI 10.1002/andp.19354160705
- 318 Cai JC, Wei W, Hu XY, Wood, DA (2017) Electrical conductivity models in saturated porous media: A 319 review. Earth-Science Reviews, 171, 419-433 DOI 10.1016/j.earscirev.2017.06.013
  - Daily W, Ramirez A, LaBrecque D, Nitao J (1992) Electrical resistivity tomography of vadose water movement. Water Resources Research 28: 1429-1442 DOI 10.1029/91wr03087
  - Datta S, Neal AW, Mohajerin TJ, Ocheltree T, Rosenheim BE, White CD, Johannesson KH (2011) Perennial ponds are not an important source of water or dissolved organic matter to groundwaters with high arsenic concentrations in West Bengal, India. Geophysical Research Letters 38 DOI 10.1029/2011gl049301
  - De Franco R, Biella G, Tosi L, Teatini P, Lozej A, Chiozzotto B, Giada M, Rizzetto F, Claude C, Mayer A (2009) Monitoring the saltwater intrusion by time lapse electrical resistivity tomography: The Chioggia test site (Venice Lagoon, Italy). Journal of Applied Geophysics 69: 117-130
  - Fetter C (1994) Applied Hydrogeology, Prentice Hall. New Jersy, NJ: 691

321

322

323

324

325

326

327

328

329

330

331

332

333

334

335

336

337

338

339

340

341

342

343

344

345

346

347

348

349

350

351

352

353

354

355

356

357

358

- Glover PWJ, Hole MJ, Pous J (2000) A modified Archie's law for two conducting phases. Earth and Planetary Science Letters 180:369-383.
- Horneman A, van Geen A, Kent DV, Mathe PE, Zheng Y, Dhar RK, O'Connell S, Hoque MA, Aziz Z, Shamsudduha M, Seddique AA, Ahmed KM (2004) Decoupling of As and Fe release to Bangladesh groundwater under reducing conditions. Part I: Evidence from sediment profiles. Geochimica et Cosmochimica Acta 68: 3459-3473 DOI 10.1016/j.gca.2004.01.026
- Hossain D (2016) Possibility of Inferring Water Quality using DC Electrical Resistivity Measurements: A Case Study of the Dupi Tila Aquifer in Bangladesh. Journal of Bangladesh Academy of Sciences 40: 1-10
- Islam M, Bashar K, Ahmed N, Rasul MG, Hossain S, Sarker MMR (2018) Hydrogeologic Characteristics and Groundwater Potentiality of Lower Aquifer of Singair Upazila, Manikgani District, Bangladesh. Journal of Bangladesh Academy of Sciences 42: 25-40
- Kabir AS, Hossain D, Abdullah R (2011) 2-D electrical imaging in some geotechnical investigation of Madhupur clays, Bangladesh. Journal of the Geological Society of India 77: 73-81
- Khaki M, Forootan E, Kuhn M, Awange J, Papa F, Shum CK (2018) A study of Bangladesh's sub-surface water storages using satellite products and data assimilation scheme. Science of The Total Environment 625: 963-977 DOI 10.1016/j.scitotenv.2017.12.289
- Knappett P, Mailloux B, Choudhury I, Khan M, Michael H, Barua S, Mondal D, Steckler M, Akhter S, Ahmed K (2016) Vulnerability of low-arsenic aquifers to municipal pumping in Bangladesh. Journal of Hydrology 539: 674-686
- Loke M (2006) RES2DINV ver. 3.55, Rapid 2D resistivity and IP inversion using the least-squares method. Software Manual 139
- Loke M (2011) Electrical Resistivity Surveys and Data Interpretation
- McArthur J, Ravenscroft P, Banerjee D, Milsom J, Hudson-Edwards KA, Sengupta S, Bristow C, Sarkar A, Tonkin S, Purohit R (2008) How paleosols influence groundwater flow and arsenic pollution: a model from the Bengal Basin and its worldwide implication. Water Resources Research 44
- Michael HA, Khan MR (2016) Impacts of physical and chemical aquifer heterogeneity on basin-scale solute transport: Vulnerability of deep groundwater to arsenic contamination in Bangladesh. Advances in Water Resources 98: 147-158 DOI 10.1016/j.advwatres.2016.10.010
- 359 Mihajlov I, Mozumder MRH, Bostick BC, Stute M, Mailloux BJ, Knappett PS, Choudhury I, Ahmed 360 KM, Schlosser P, van Geen A (2020) Arsenic contamination of Bangladesh aquifers exacerbated by clay layers. Nature communications 11: 1-9
- 362 Mozumder M, Michael H, Mihajlov I, Khan M, Knappett P, Bostick B, Mailloux B, Ahmed K, 363 Choudhury I, Koffman T (2020) Origin of groundwater arsenic in a rural Pleistocene aquifer in 364 Bangladesh depressurized by distal municipal pumping. Water Resources Research: 365 e2020WR027178

- Najman Y, Bickle M, BouDagher-Fadel M, Carter A, Garzanti E, Paul M, Wijbrans J, Willett E, Oliver G, Parrish R, Akhter SH, Allen R, Ando S, Chisty E, Reisberg L, Vezzoli G (2008) The Paleogene record of Himalayan erosion: Bengal Basin, Bangladesh. Earth and Planetary Science Letters 273: 1-14 DOI 10.1016/j.epsl.2008.04.028
- Nickson R, McArthur J, Burgess W, Ahmed KM, Ravenscroft P, Rahmanñ M (1998) Arsenic poisoning
   of Bangladesh groundwater. Nature 395: 338-338 DOI 10.1038/26387
   Nowroozi AA, Horrocks SB, Henderson P (1999) Saltwater intrusion into the freshwater aquifer in the

- Nowroozi AA, Horrocks SB, Henderson P (1999) Saltwater intrusion into the freshwater aquifer in the eastern shore of Virginia: a reconnaissance electrical resistivity survey. Journal of Applied Geophysics 42: 1-22 DOI 10.1016/S0926-9851(99)00004-X
- Pearson CF, Halleck PM, McGuire PL, Hermes R, Mathews M (1983) Natural gas hydrate deposits: a review of in situ properties. The Journal of Physical Chemistry 87: 4180-4185 DOI 10.1021/j100244a041
- Waxman MH, Smits LJM (1968) Electrical conductivities in oil-bearing shaly sands. Society of Petroleum Engineers Journal 8:107-122.
- Wang H, Revil A (2020) Surface conduction model for fractal porous media. Geophysical Research Letters 47: e2020GL087553.
- Wilson C, Goodbred S (2015) Construction and maintenance of the Ganges-Brahmaputra-Meghna Delta: Linking process, morphology, and stratigraphy. Annual Review of Marine Science 7 DOI 10.1146/annurev-marine-010213-135032
- Woobaidullah A, Chowdhury SH, Ahmed KM, Rahman MW, Arafin KS, Al-Ejaz O (2008) Geo-electric Resistivity Survey in the Evaluation of Hydrogeological Condition in Haziganj Upazila, Chandpur District, Bangladesh. Journal of the Geological Society of India 72: 753-763
- Zahid A, Ahmed SRU (2006) Groundwater resources development in Bangladesh: Contribution to irrigation for food security and constraints to sustainability. Groundwater Governance in Asia Series-1: 25-46

# 392 Figures and Tables

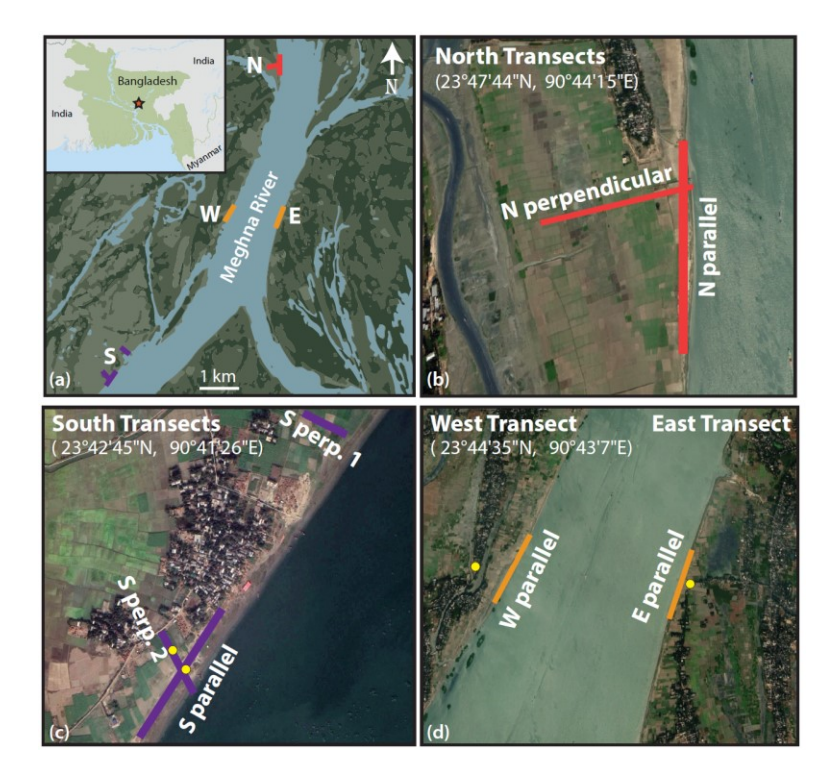


**Fig 1.** Overview of the study region (a) and locations of electrical resistivity imaging transects (b-d). The yellow circles denote boreholes where sediment grainsize and/or pore fluid resistivity were observed. The coordinates indicate the approximate center of each image. Images were taken from Google Earth.

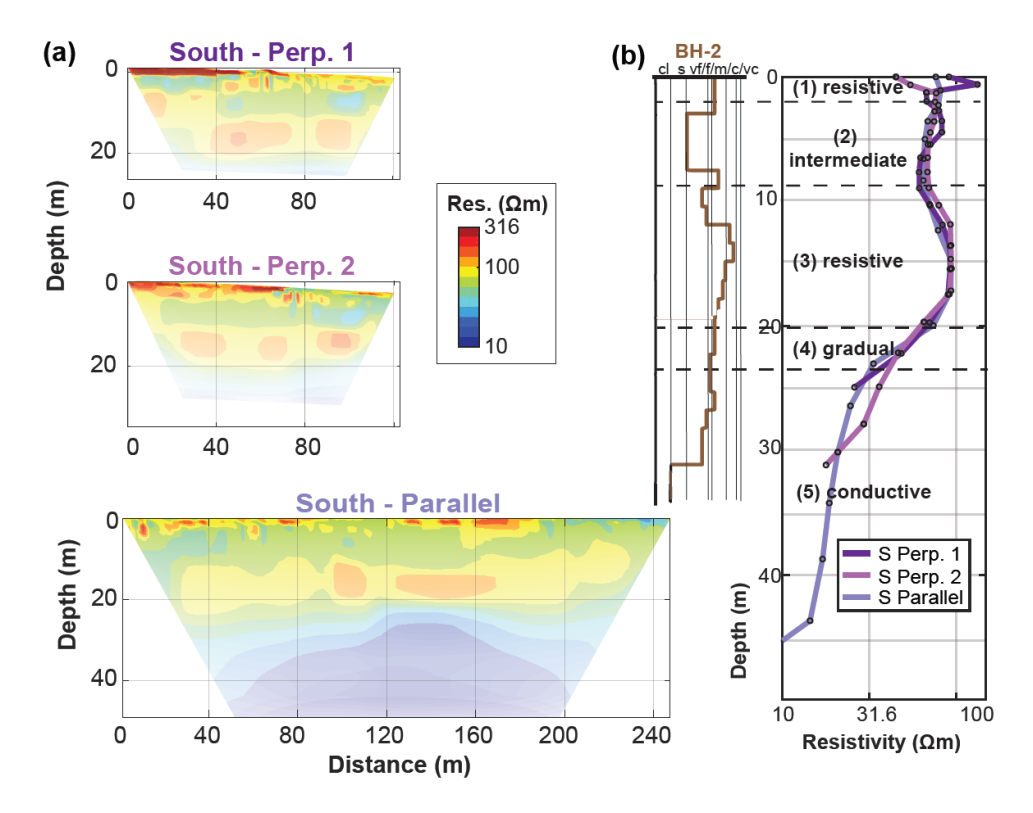


**Fig 2.** (a) Resulting electrical resistivity tomograms and comparison with borehole data from the South transects. (b) Grainsize for cuttings from a nearby borehole (BH-2) and vertical resistivity profiles extracted from the middle of each resistivity survey (right). In (b), the grainsize categories are clay, silt, and very fine to coarse sand from left to right, respectively. The transparency of the tomograms reflects the model resolution decreasing with depth.

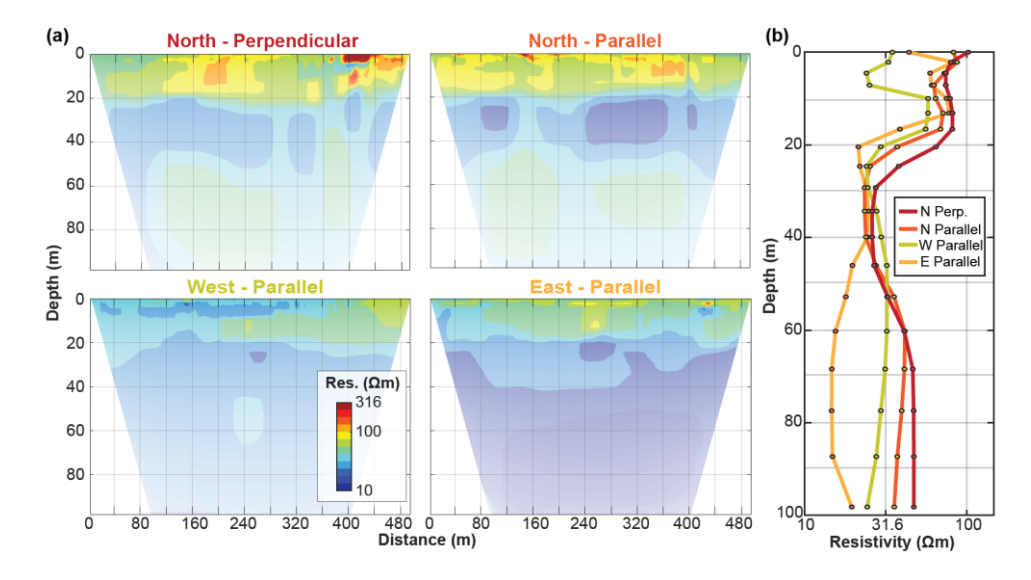


**Fig. 3**. (a) Electrical resistivity tomograms and (b) vertical profiles extracted from the middle of each survey shown down to their full depth extent for the North, West, and East transects. The locations of the transects are shown in Fig. 1b and d. The transparency of the tomograms reflects the model resolution decreasing with depth.

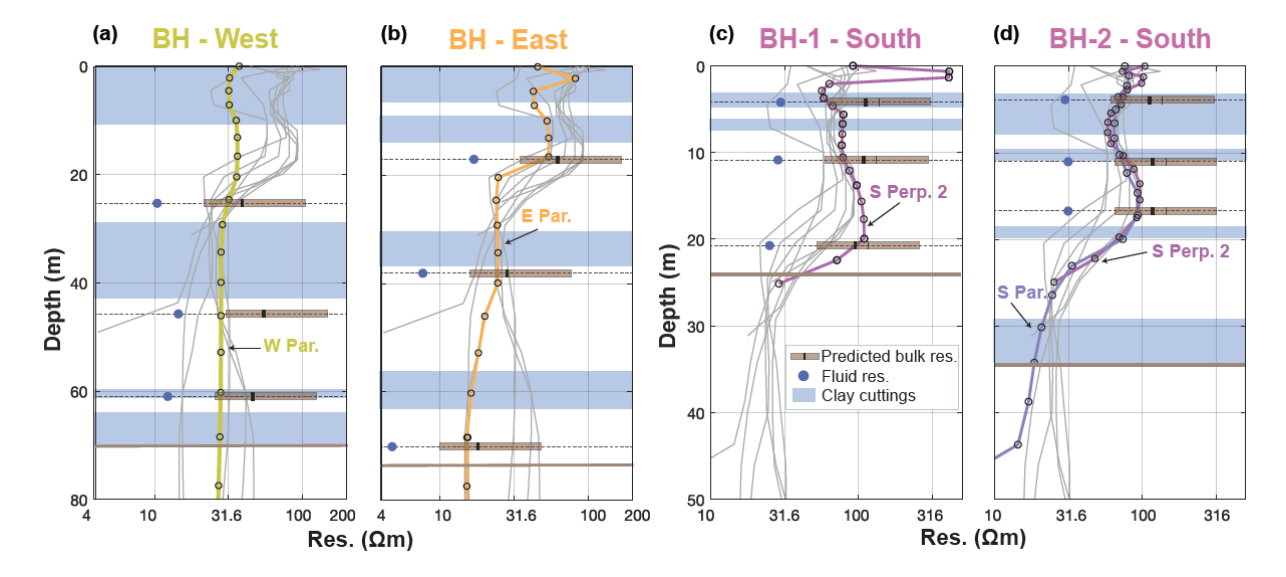


**Fig 4.** Comparison of extracted vertical bulk electrical resistivity (ER) profiles from the tomograms with measured pore fluid resistivity and predicted bulk resistivity. A series of vertical ER profiles taken at equal horizontal distances across the tomograms are denoted by gray lines whereas the profile closest to the borehole (BH) is colored. The predicted bulk resistivity range, calculated using Archie's Law, is

indicated by the brown bar with the median value denoted by the bold line. A porosity range of 20-60% and the measured fluid resistivity (blue circles) were assumed. Intervals with sediment finer than fine sand (i.e., very fine sand, silt and clay) are highlighted by the light blue shaded boxes. The borehole locations are shown in Fig. 1. BH-1 and BH-2 are along the South perpendicular 2 transect, with BH-1 to the west. The water table is no deeper than 2 m below ground surface.



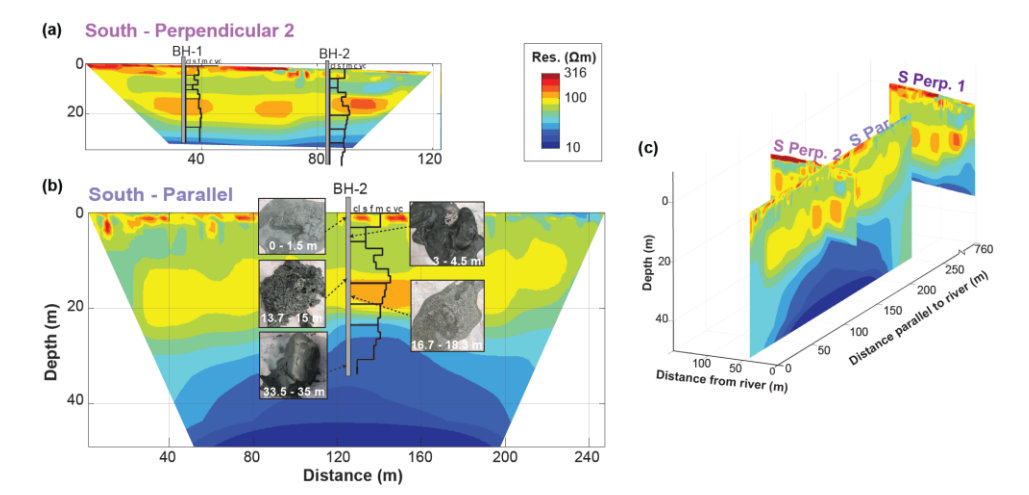


**Fig 5.** (a) shows the superposed images of tomograms, borehole grainsize data and wet-sediment colors of core cuttings for the South transects. (b) shows the three-dimensional configuration and relationship of the tomograms.

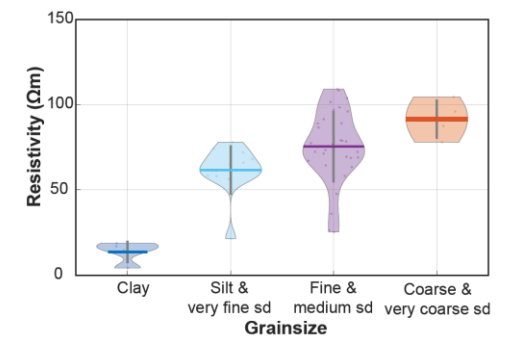


**Fig 6.** Comparison of grainsize visually observed from borehole cuttings with bulk resistivity values for borehole locations for the South site. The comparison only includes observations below the water table. The violin plots show the relative density of data points for each grainsize grouping and highlight the mean (horizontal line) and interquartile range (vertical line).

# when running when constructing and implementing the inversion in RES2DINV.

Inversion parameter or property	Setting	
Numerical model type	Finite-element	
Inversion method	Robust inversion using L1 Norm	
Robust data cut-off factor	0.05	
Nodes	4	
Initial damping factor	0.15	
Minimum damping factor	0.02	
V/H filter ratio	1	
Model block discretization	Same width with reduced edge effects	
Mesh size	Finest mesh grid size	
Limit resistivities	None	
Iterations	<6	
Convergence limit for rel. change in %RMS	5%	

**Table 2.** Apparent resistivity and inversion data. Outliers with apparent resistivity greater than 100,000  $\Omega m$  or lower than 0.01  $\Omega m$  were removed; the number of points removed are in parentheses. The minimum, maximum and mean apparent resistivity values are included for each survey. The RMS error for each inversion is also included.

Survey	Number of measurements	RMS (%)	Min., max., and mean app. res. (Ωm)
South Perp. 1	4247 (4)	1.6	20.3, 1903.3, 76.3
South Perp. 2	3215 (0)	3.9	0.2, 1355.4, 88.7
South Parallel	3141 (21)	8.5	0.15, 3192.9, 28.9
East Parallel	3248 (1)	1.0	14.6, 115.6, 30.3
West Parallel	3248 (2)	1.9	10.2, 66.9, 33.7
North Parallel	3248 (0)	3.4	4.3, 122.0, 46.6
North Perp.	3248 (0)	1.8	14.7, 823.2, 50.3

**Table 3.** Resulting p values of t-tests for comparing the resistivity of zones with different grainsize classes. The p value indicates the likelihood of accepting the hypothesis that the grain size groupings have different means when there is actually no difference. All p values are <0.1 (10% significance level) and most are <0.05 (5% significance level). The data used in the analysis correspond to those shown in Fig. 6.

Grainsize class	Clay	Silt & v. fine sand	Fine & med. sand	Coarse & v. coarse sand
Clay	-	9.0×10 <sup>-7</sup>	7.5×10 <sup>-9</sup>	9.9×10 <sup>-5</sup>
Silt & v. fine sand	9.0×10 <sup>-7</sup>	-	0.019	0.004
Fine & med. sand	7.5×10 <sup>-9</sup>	0.019	-	0.054
Coarse & v. coarse sand	9.9×10 <sup>-5</sup>	0.004	0.054	-